by the discrete form of (83), i.e.,

$$D(n) = \left(\frac{d\phi(n)}{dn}\right)^2 = \Omega_i^2(n) = (\Omega_c + \Omega_m \cos(\Omega_f n))^2$$

$$E(n) = \frac{d^2\phi(n)}{dn^2}\frac{\sin(2\phi(n))}{2}$$
$$= -\frac{\Omega_m\Omega_f}{2}\sin(\Omega_f n)\sin\left(2\left(\Omega_c n + \frac{\Omega_m}{\Omega_f}\sin(\Omega_f n)\right)\right)$$

and

$$|E(n)| \le \frac{\Omega_m\Omega_f}{2}. \tag{1}$$

Note that there are no constraints on Ω_f, and clearly, $|E(n)|$ increases as Ω_f increases. In addition, it is obvious that $|E(n)| = 0$ when $\Omega_f = 0$. Of course, this is intuitively appealing since one would hope that frequency tracking of a constant frequency sinusoidal signal ($\Omega_f = 0$) would be very accurate ($|E| = 0$). However, this does not agree with Proposition 3 [1, p. 1542]. In the proof of this proposition, the following is given:

$$|E| \le \beta\left[2 - \sqrt{2}\sin\left(\Omega_f + \frac{\pi}{4}\right)\right] \le \beta$$

or

$$|E| \le \frac{\Omega_m}{\Omega_f}.$$

This is inconsistent with (1) and counter intuitive (at least to us). Why are these so different? A close examination of (102) will answer this question and reveals the error in the Proof of Proposition 3.

$$A + \phi = \Omega_c n + \beta\cos(\Omega_f)\sin(\Omega_f n) + \theta + \Omega_c n + \beta\sin(\Omega_f n) + \theta$$
$$A - \phi = \Omega_c n + \beta\cos(\Omega_f)\sin(\Omega_f n) + \theta - \Omega_c n - \beta\sin(\Omega_f n) - \theta$$
$$B + \Omega_i = \Omega_c + \beta\sin(\Omega_f)\cos(\Omega_f n) + \Omega_c + \Omega_m\cos(\Omega_f n)$$
$$B - \Omega_i = \Omega_c + \beta\sin(\Omega_f)\cos(\Omega_f n) - \Omega_c - \Omega_m\cos(\Omega_f n)$$
$$= \beta\sin(\Omega_f)\cos(\Omega_f n) - \beta\Omega_f\cos(\Omega_f n)$$

and

$$A - \phi = \beta\sin(\Omega_f n)(\cos(\Omega_f) - 1)$$
$$B - \Omega_i = \beta\cos(\Omega_f n)(\sin(\Omega_f) - \Omega_f).$$

This last equation is most likely where the error occurred since the proof contains a term $\sin(\gamma_2)$ with $\gamma_2 = \beta[1 - \sin(\Omega_f)]$.

Now, if we proceed as in the paper

$$|E| \le \beta(1 - \cos(\Omega_f)) + \beta(\Omega_f - \sin(\Omega_f))$$

or replacing β with Ω_m/Ω_f and rearranging terms

$$|E| \le \Omega_m\left[\frac{(\Omega_f + 1) - (\cos(\Omega_f) + \sin(\Omega_f))}{\Omega_f}\right] \tag{2}$$

and with the help of L'Hospital's rule, it follows that

$$\lim_{\Omega_f \to 0}|E| = 0$$

which is satisfying. It is interesting to compare this upperbound on $|E|$ to the one given by (1) for $\Omega_f \le \pi/2$.

We hope that this will be helpful to others in the analysis of this interesting paper.

REFERENCES

[1] P. Maragos, J. F. Kaiser and T. F. Quatieri, "On amplitude and frequency demodulation using energy operators," *IEEE Trans. Signal Processing*, vol. 41, pp. 1532–1550, Apr. 1993.

Structures for Anticausal Inverses and Application in Multirate Filter Banks

P. P. Vaidyanathan and Tsuhan Chen

***Abstract*— Anticausal or time-reversed inversion of digital filters has gained importance in recent years in the implementation of digital filter banks. Anticausal inversion has, in the past, been shown to be possible by using block processing with appropriate state initialization. With (A, B, C, D) denoting the state space description of a structure implementing a filter $G(z)$, the anticausal inverse can be essentially regarded as a filter structure having an inverted state-space description, which we denote as ($\hat{A}$, $\hat{B}$, $\hat{C}$, $\hat{D}$). It is usually not efficient to implement the state space equations given by ($\hat{A}$, $\hat{B}$, $\hat{C}$, $\hat{D}$) directly because of excessive multiplier count. Rather, one seeks to find an efficient structure having the inverse description ($\hat{A}$, $\hat{B}$, $\hat{C}$, $\hat{D}$). While this can be done by inspection in simple cases such as the direct-form structure, systematic procedures for other important structures have yet to be developed. In this correspondence, we derive anticausal inverse structures corresponding to several standard IIR filter structures such as the direct-form, cascade-form, coupled-form, and the entire family of IIR lattice structures including the tapped cascaded lattice. We introduce the notion of a *causal dual*, which we find convenient in the derivations. We show that the limit-cycle free property of the original structure is inherited by the causal dual in some but not all cases.**

I. INTRODUCTION

Anticausal inversion of IIR transfer functions has gained some importance in recent years in the implementation of digital filter banks. This was first motivated by a class of two-channel filter banks (Fig. 1), where the analysis and synthesis filters are derived from causal stable allpass filters $a_i(z)$ as [1], [2]

$$H_0(z) = \frac{a_0(z^2) + z^{-1}a_1(z^2)}{2}$$
$$H_1(z) = \frac{a_0(z^2) - z^{-1}a_1(z^2)}{2}$$
$$F_0(z) = H_0(z), \quad F_1(z) = -H_1(z). \tag{1}$$

The system can, therefore, be redrawn as shown in Fig. 2(a) [1]–[3]. This system is free from aliasing, and the output is $\hat{X}(z) = T(z)X(z)$, where $T(z) = 0.5z^{-1}a_0(z^2)a_1(z^2)$. Thus, the distortion function is allpass, and the system suffers only from phase distortion created by $a_0(z^2)a_1(z^2)$. It was suggested by Ramstad [2] that we can eliminate this phase distortion and thereby obtain perfect reconstruction (i.e., $\hat{x}(n) = x(n)$) simply by modifying the synthesis bank as shown in Fig. 2(b). However, since $a_i(z)$ are stable allpass

Manuscript received February 21, 1995; revised August 26, 1997. This work was supported in part by Office of Naval Research Grant N00014-93-1-0231, Tektronix, Inc., and Rockwell International.

P. P. Vaidyanathan is with the Department of Electrical Engineering, California Institute of Technology, Pasadena, CA 91125 USA.

T. Chen is with the Department of Electrical Engineering, Carnegie Mellon University, Pittsburgh, PA 15213 USA.

Publisher Item Identifier S 1053-587X(98)01341-5.

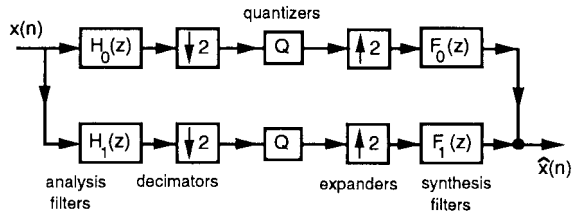

Fig. 1. Two-channel maximally decimated filter bank.

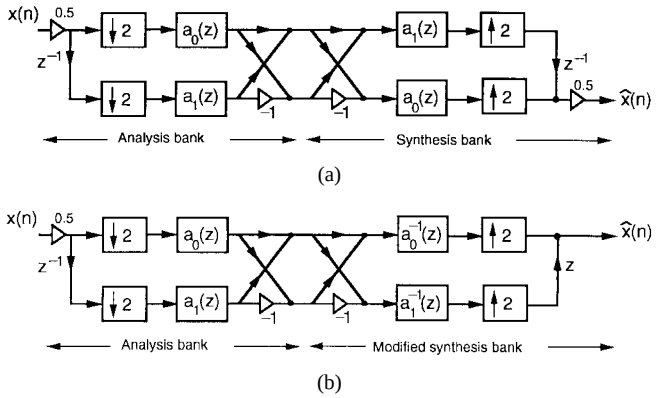

Fig. 2. (a) Allpass-based filter bank. (b) Modified version having the perfect reconstruction property.

filters with poles inside the unit circle, their reciprocals $1/a_i(z)$ have poles outside the unit circle [4], resulting in unstable synthesis filters. Husoy and Ramstad proposed [2], [5] that this difficulty can be overcome by implementing $1/a_i(z)$ as anticausal filters because anticausal filters with poles outside the unit circle are stable [4]. It was later shown by Babic *et al.* [6] that this anticausal or time-reversed inversion works as long as we carefully select the initial conditions in the time-reversed difference equations. Even with infinitely long inputs, this idea works perfectly in a block-by-block manner, provided we accept a finite latency [7].

A general state space theory for time reversed (or anticausal) inversion of linear systems was then proposed in [8] and [9] and has also been applied to M-channel filter banks. Thus, consider a causal stable Nth-order digital filter $G(z)$ implemented using some structure (e.g., direct-form, lattice, ...). Assume that the structure is minimal (i.e., it has just N delay elements z^{-1}). Defining the outputs of the delay elements as the state variables $x_i(n)$, we can obtain a state-space description $(\boldsymbol{A}, \boldsymbol{B}, \boldsymbol{C}, D)$ (e.g., see [3, Sec. 13.4])

$$\begin{bmatrix} \boldsymbol{x}(n+1) \\ y(n) \end{bmatrix} = \underbrace{\begin{bmatrix} \boldsymbol{A} & \boldsymbol{B} \\ \boldsymbol{C} & D \end{bmatrix}}_{\mathcal{R}} \begin{bmatrix} \boldsymbol{x}(n) \\ u(n) \end{bmatrix} \tag{2}$$

where $\mathcal{R}$ is said to be the *realization matrix* of the implementation. Here, $\boldsymbol{x}(n) = [x_1(n) \ \cdots \ x_N(n)]^T$ is the state vector, $u(n)$ the filter input, and $y(n)$ the filter output. $\boldsymbol{A}$ is $N \times N$, $\boldsymbol{B}$ is $N \times 1$, $\boldsymbol{C}$ is $1 \times N$, and D is a scalar. If all the poles of $1/G(z)$ are outside the unit circle, we can obtain an anticausal stable impulse response. To see how it can be implemented, imagine that we start the system (2) with the initial state $\boldsymbol{x}(0)$ and apply the causal input $u(n)$, possibly of infinite duration. Consider a segment of L input samples $u(0), u(1), \cdots, u(L-1)$, where L is an arbitrary integer. Denote the output during this period as $y(0), y(1), \cdots, y(L-1)$. The final state-vector $\boldsymbol{x}(L)$ and the above segment of the output are completely determined by the input segment and initial state-vector $\boldsymbol{x}(0)$. By observing $\boldsymbol{x}(L)$ and the above finite segment of the output, we can reconstruct the input segment and the initial state $\boldsymbol{x}(0)$ if $\mathcal{R}$ is nonsingular.[1] Thus, define

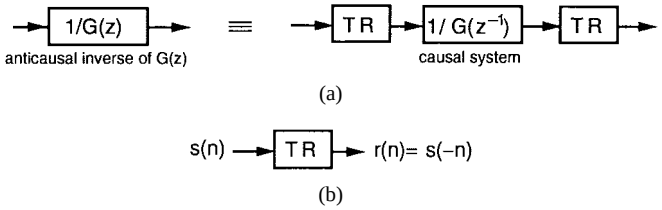

Fig. 3. (a) Anticausal inverse represented in terms of a causal system and time-reversal operators. (b) Meaning of the time-reversal operator.

$$\hat{\mathcal{R}} \triangleq \begin{bmatrix} \hat{\boldsymbol{A}} & \hat{\boldsymbol{B}} \\ \hat{\boldsymbol{C}} & \hat{D} \end{bmatrix} = \begin{bmatrix} \boldsymbol{A} & \boldsymbol{B} \\ \boldsymbol{C} & D \end{bmatrix}^{-1}. \tag{3}$$

Consider the causal system described by the inverse state space description $(\hat{\boldsymbol{A}}, \hat{\boldsymbol{B}}, \hat{\boldsymbol{C}}, D)$, namely

$$\begin{bmatrix} \hat{\boldsymbol{x}}(n+1) \\ \hat{y}(n) \end{bmatrix} = \underbrace{\begin{bmatrix} \hat{\boldsymbol{A}} & \hat{\boldsymbol{B}} \\ \hat{\boldsymbol{C}} & \hat{D} \end{bmatrix}}_{\hat{\mathcal{R}}} \begin{bmatrix} \hat{\boldsymbol{x}}(n) \\ \hat{u}(n) \end{bmatrix}. \tag{4}$$

If we run this by setting the initial state to be $\hat{\boldsymbol{x}}(L) = \boldsymbol{x}(L)$ and the input to be $\hat{u}(L+k) = y(L-1-k), 0 \le k \le L-1$, then the output for this duration will be $\hat{y}(L+k) = u(L-1-k), 0 \le k \le L-1$, and the final state will be $\hat{\boldsymbol{x}}(2L) = \boldsymbol{x}(0)$. Since $\hat{y}(2L-1) = u(0)$, the latency is $2L-1$ samples. By repeating this process in a block-by-block manner, we can implement the anticausal inverse $1/G(z)$ of the original filter $G(z)$. This works for IIR filters, IIR inverses, and infinitely long inputs. The transfer function of the system (4) is $\hat{Y}(z)/\hat{U}(z) = \hat{D} + \hat{\boldsymbol{C}}(z\boldsymbol{I} - \hat{\boldsymbol{A}})^{-1}\hat{\boldsymbol{B}}$. Rewriting (4) in terms of $(\boldsymbol{A}, \boldsymbol{B}, \boldsymbol{C}, D)$, we verify $\hat{U}(z)/\hat{Y}(z) = D + \boldsymbol{C}(z^{-1}\boldsymbol{I} - \boldsymbol{A})^{-1}\boldsymbol{B} = G(z^{-1})$. Therefore, the causal systems (2) and (4) have transfer functions

$$\begin{aligned} G(z) &= D + \boldsymbol{C}(z\boldsymbol{I} - \boldsymbol{A})^{-1}\boldsymbol{B} \\ 1/G(z^{-1}) &= \hat{D} + \hat{\boldsymbol{C}}(z\boldsymbol{I} - \hat{\boldsymbol{A}})^{-1}\hat{\boldsymbol{B}} \end{aligned} \tag{5}$$

respectively. If $1/G(z)$ is anticausal stable, then $1/G(z^{-1})$ is causal stable, and the eigenvalues of $\hat{\boldsymbol{A}}$ are inside the unit circle. Ideally, the anticausal transfer function $1/G(z)$ is related to $1/G(z^{-1})$ in terms of ideal time reversal (TR) operators, as shown schematically in Fig. 3. In practice, we replace the TR operators with blockwise time reversal as described above and implement the sandwiched causal component $1/G(z^{-1})$ by using the causal state space recursion (4) with appropriate initial conditioning for each block.

The filter $1/G(z^{-1})$ can, in principle, be implemented using any one of an infinite number of possible structures (direct-form, cascade-form, lattice, and so forth). Not all these structures will have the inverse state space description $(\hat{\boldsymbol{A}}, \hat{\boldsymbol{B}}, \hat{\boldsymbol{C}}, \hat{D})$, even though they are related to $(\hat{\boldsymbol{A}}, \hat{\boldsymbol{B}}, \hat{\boldsymbol{C}}, \hat{D})$ by similarity transformations. Thus, if an arbitrary structure is used for $1/G(z^{-1})$, then the initialization of the state for each input block of length L should be done only after a state transformation at the beginning of each block.

The aim of this correspondence is to find a structure for $1/G(z^{-1})$ that has precisely the inverse state space description $(\hat{\boldsymbol{A}}, \hat{\boldsymbol{B}}, \hat{\boldsymbol{C}}, \hat{D})$ Such a structure for $1/G(z^{-1})$ will be called the *causal dual* of the original structure $(\boldsymbol{A}, \boldsymbol{B}, \boldsymbol{C}, D)$. We also say that $(\hat{\boldsymbol{A}}, \hat{\boldsymbol{B}}, \hat{\boldsymbol{C}}, \hat{\boldsymbol{D}})$ is the *inverse state space description*. The initial state vector for $(\hat{\boldsymbol{A}}, \hat{\boldsymbol{B}}, \hat{\boldsymbol{C}}, \hat{\boldsymbol{D}})$ at the beginning of each block is precisely the state vector of $(\boldsymbol{A}, \boldsymbol{B}, \boldsymbol{C}, D)$ at the end of the preceding block. *No similarity transformations are necessary.* To illustrate, consider the direct-form

[1] Nonsingularity of $\mathcal{R}$ is necessary and sufficient for existence of an anticausal inverse [9].

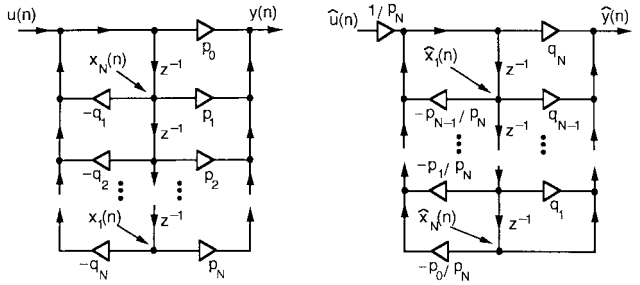

Fig. 4. (a) General direct-form structure. (b) Its causal dual.

structure for the transfer function $G(z) = \Sigma_{n=0}^{N} p_n z^{-n}/(1 + \Sigma_{n=1}^{N} q_n z^{-n})$ shown in Fig. 4(a). The inverse filter $1/G(z)$ has an anticausal impulse response (more simply, $G(z)$ has an anticausal inverse) if and only if $p_N \neq 0$ [9]. With the state variables $x_i(n)$ as indicated in the figure, the state transition matrix $\boldsymbol{A}$ is in companion form (e.g., see [3]), and the realization matrix is

$$\mathcal{R} = \begin{bmatrix} \boldsymbol{A} & \boldsymbol{B} \\ \boldsymbol{C} & D \end{bmatrix} = \begin{bmatrix} 0 & 1 & \cdots & 0 & 0 \\ 0 & 0 & \cdots & 0 & 0 \\ \vdots & & \ddots & \vdots & \\ 0 & 0 & \cdots & 1 & 0 \\ -q_N & -q_{N-1} & \cdots & -q_1 & 1 \\ p_N - p_0 q_N & p_{N-1} - p_0 q_{N-1} & \cdots & p_1 - p_0 q_1 & p_0 \end{bmatrix}. \quad (6)$$

The inverse of this matrix is

$$\hat{\mathcal{R}} = \mathcal{R}^{-1} = \begin{bmatrix} -p_{N-1}/p_N & \cdots & -p_1/p_N & -p_0/p_N & 1/p_N \\ 1 & \cdots & 0 & 0 & 0 \\ \vdots & \ddots & & \vdots & \vdots \\ 0 & \cdots & 1 & 0 & 0 \\ r_0 & \cdots & r_{N-2} & r_{N-1} & q_N/p_N \end{bmatrix} \quad (7)$$

where $r_i = q_{N-i-1} - (q_N p_{N-i-1}/p_N), 0 \leq i \leq N-1$. It can be verified that the structure shown in Fig. 4(b), with the state variables numbered as indicated, has the above realization matrix and is therefore the causal dual of the direct form. To obtain the causal dual, we, therefore, do the following.

1) Replace the feedforward multipliers p_i by the feedback multipliers q_i (with $q_0 \triangleq 1$) but in reverse order.
2) Replace the feedback multipliers $-q_i$ with $-p_i/p_N$, again in reverse order, and insert a scale factor $1/p_N$ at the input.
3) Renumber the state variables in reverse order.

When we transfer the final state of the structure $(\boldsymbol{A}, \boldsymbol{B}, \boldsymbol{C}, D)$ to the initial state of $(\hat{\boldsymbol{A}}, \hat{\boldsymbol{B}}, \hat{\boldsymbol{C}}, \hat{D})$ at the end of every block, we have to keep in mind this renumbering. The contents of the top delay in Fig. 4(a) should be transferred to the bottom delay in Fig. 4(b), and so forth. This was first observed in [10]. For the special case of *allpass* filters with real coefficients, it follows that the causal dual is identical to the original structure—*only the states need to be renumbered.*

A trivial way to find the causal dual is to build a structure with multiplier coefficients equal to the elements in $(\hat{\boldsymbol{A}}, \hat{\boldsymbol{B}}, \hat{\boldsymbol{C}}, \hat{D})$. For arbitrary structures, this requires $(N+1)^2$ multipliers. In Sections II–IV, we derive the causal duals for the cascade-form, coupled-form, and lattice structures and show that, at least for these popular structures, the number of multipliers in the causal dual is proportional to N rather than N^2.

It is well known that the coupled-form and lattice structures satisfy a sufficient condition for absence of limit cycles, which are called (generalized) passivity [11], [13]. In general, if $(\boldsymbol{A}, \boldsymbol{B}, \boldsymbol{C}, D)$ satisfies such a condition, this does not imply that the causal dual $(\hat{\boldsymbol{A}}, \hat{\boldsymbol{B}}, \hat{\boldsymbol{C}}, \hat{D})$ also satisfies it, as demonstrated in Section V of this correspondence for the case of the coupled-form allpass structure. However, all popular allpass lattice structures are such that the casual duals are also generalized passive (Section V).

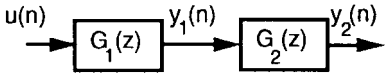

Fig. 5. Pertaining to anticausal inversion of a cascaded system.

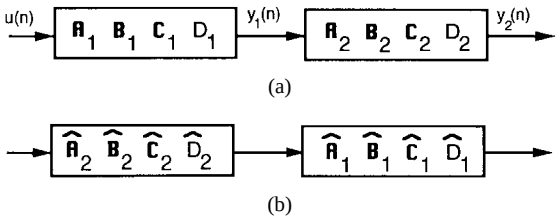

Fig. 6. (a) General cascade. (b) Its causal dual.

II. Causal Duals for Cascaded Structures

Consider a cascade of causal filters $G_1(z)$ and $G_2(z)$ (Fig. 5). To obtain an anticausal inverse, one chooses a convenient block length L. Then, from the block of L outputs $y_2(n) \cdots y_2(n+L-1)$ and the state $\boldsymbol{x}_2(n+L)$ of $G_2(z)$, we can recover the block of L inputs $y_1(n) \cdots y_1(n+L-1)$ of the system $G_2(z)$. We can then use $y_1(n) \cdots y_1(n+L-1)$ [output block of $G_1(z)$] and the state vector $\boldsymbol{x}_1(n+L)$ of the system $G_1(z)$ to recover the primary input block $u(n) \cdots u(n+L-1)$. This is equivalent to connecting the anticausal inverses in reverse order. In fact, we can simplify this result further. Fig. 6(a) shows the state space descriptions of the two structures given by $(\boldsymbol{A}_1, \boldsymbol{B}_1, \boldsymbol{C}_1, D_1)$ and $(\boldsymbol{A}_2, \boldsymbol{B}_2, \boldsymbol{C}_2, D_2)$. Let their causal duals be, respectively, $(\hat{\boldsymbol{A}}_1, \hat{\boldsymbol{B}}_1, \hat{\boldsymbol{C}}_1, \hat{D}_1)$ and $(\hat{\boldsymbol{A}}_2, \hat{\boldsymbol{B}}_2, \hat{\boldsymbol{C}}_2, \hat{D}_2)$. Then, the causal dual of the cascade is as shown in Fig. 6(b). That is, it is the cascade of the individual causal duals in reversed order. Thus, we can implement the causal cascaded structure for $1/G(z^{-1})$ and use blockwise time reversal of its primary input and output to obtain the anticausal implementation of the inverse $1/G(z)$; time reversal is necessary only at the primary input and output nodes. To verify that Fig. 6(b) is indeed the causal dual, note that the state space description for the cascaded system with input $u(n)$, output $y_2(n)$, and extended state vector $\begin{bmatrix} \boldsymbol{x}_1(n) \\ \boldsymbol{x}_2(n) \end{bmatrix}$ is

$$\begin{bmatrix} \boldsymbol{x}_1(n+1) \\ \boldsymbol{x}_2(n+1) \\ y_2(n) \end{bmatrix} = \underbrace{\begin{bmatrix} \boldsymbol{A}_1 & \boldsymbol{0} & \boldsymbol{B}_1 \\ \boldsymbol{B}_2\boldsymbol{C}_1 & \boldsymbol{A}_2 & \boldsymbol{B}_2 D_1 \\ D_2\boldsymbol{C}_1 & \boldsymbol{C}_2 & D_2 D_1 \end{bmatrix}}_{\mathcal{R}} \begin{bmatrix} \boldsymbol{x}_1(n) \\ \boldsymbol{x}_2(n) \\ u(n) \end{bmatrix}. \quad (8)$$

The matrix $\mathcal{R}$ indicated above is therefore the realization matrix of the cascade. By using the fact that $\begin{bmatrix} \boldsymbol{A}_i & \boldsymbol{B}_i \\ \boldsymbol{C}_i & D_i \end{bmatrix} \begin{bmatrix} \hat{\boldsymbol{A}}_i & \hat{\boldsymbol{B}}_i \\ \hat{\boldsymbol{C}}_i & \hat{D}_i \end{bmatrix} = \boldsymbol{I}$, we can evaluate $\mathcal{R}^{-1}$ and obtain the following description of the causal dual.

$$\begin{bmatrix} \hat{\boldsymbol{x}}_1(n+1) \\ \hat{\boldsymbol{x}}_2(n+1) \\ \hat{y}(n) \end{bmatrix} = \underbrace{\begin{bmatrix} \hat{\boldsymbol{A}}_1 & \hat{\boldsymbol{B}}_1\hat{\boldsymbol{C}}_2 & \hat{\boldsymbol{B}}_1\hat{D}_2 \\ \boldsymbol{0} & \hat{\boldsymbol{A}}_2 & \hat{\boldsymbol{B}}_2 \\ \hat{\boldsymbol{C}}_1 & \hat{D}_1\hat{\boldsymbol{C}}_2 & \hat{D}_1\hat{D}_2 \end{bmatrix}}_{\mathcal{R}^{-1}} \begin{bmatrix} \hat{\boldsymbol{x}}_1(n) \\ \hat{\boldsymbol{x}}_2(n) \\ \hat{u}(n) \end{bmatrix}$$

i.e.,

$$\begin{bmatrix} \hat{\boldsymbol{x}}_2(n+1) \\ \hat{\boldsymbol{x}}_1(n+1) \\ \hat{y}(n) \end{bmatrix} = \begin{bmatrix} \hat{\boldsymbol{A}}_2 & \boldsymbol{0} & \hat{\boldsymbol{B}}_2 \\ \hat{\boldsymbol{B}}_1\hat{\boldsymbol{C}}_2 & \hat{\boldsymbol{A}}_1 & \hat{\boldsymbol{B}}_1\hat{D}_2 \\ \hat{D}_1\hat{\boldsymbol{C}}_2 & \hat{\boldsymbol{C}}_1 & \hat{D}_1\hat{D}_2 \end{bmatrix} \begin{bmatrix} \hat{\boldsymbol{x}}_2(n) \\ \hat{\boldsymbol{x}}_1(n) \\ \hat{u}(n) \end{bmatrix}.$$

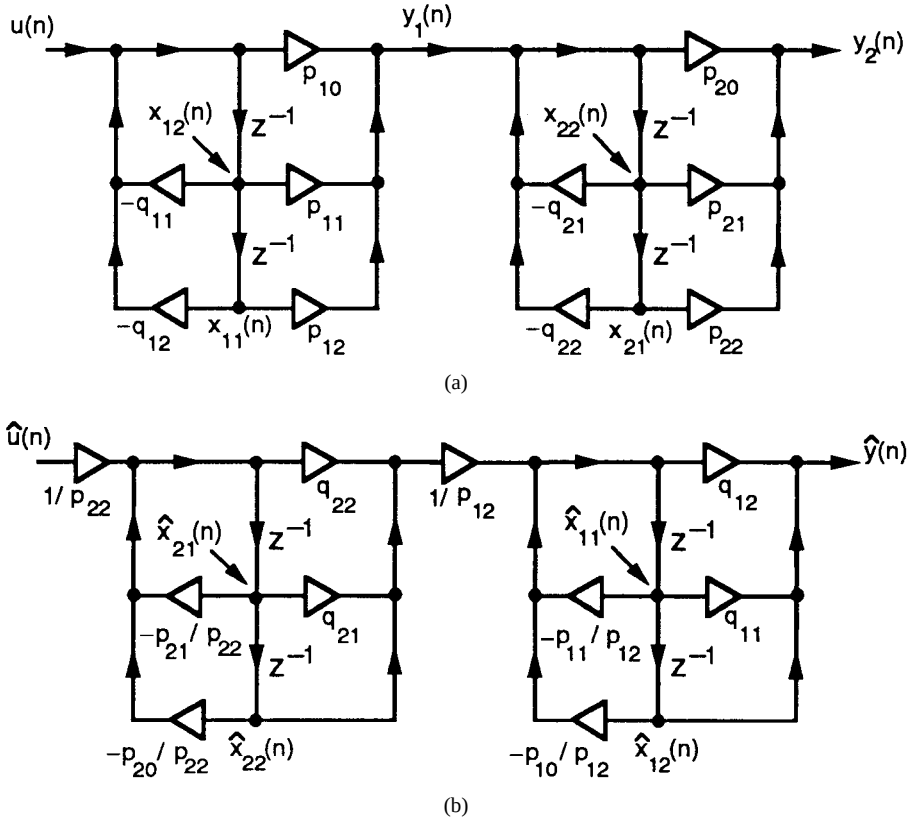

Fig. 7. (a) Cascade form example. (b) Its causal dual.

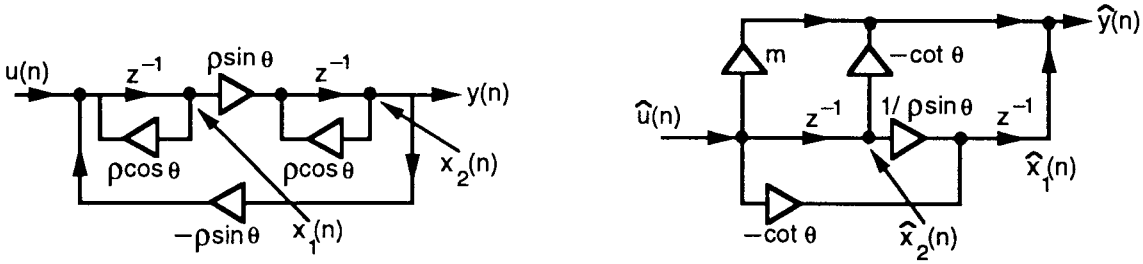

Fig. 8. (a) Coupled-form structure. (b) Its causal dual.

This resembles (8), but the subscripts 1 and 2 have been interchanged, indicating reverse ordering.

Example: Fig. 7 shows the cascade-form structure and its causal dual when the individual sections are in second-order direct form. Two points should be noted. First, the sections have to be interchanged, and second, the state variables within each direct-form section have to be renumbered in reverse order.

III. Causal Dual of the Coupled-Form

Fig. 8(a) shows the coupled form structure, whose robustness to quantization (e.g., low sensitivity and freedom from limit cycles) is well known [4], [13], [14]. The poles of this system are at $\rho e^{j\theta}$ and $\rho e^{-j\theta}$. With the output node $y(n)$ as indicated, the numerator is $\rho \sin\theta z^{-2}$. The transfer function is $G(z) = \rho \sin\theta z^{-2}/(1 - 2\rho\cos\theta z^{-1} + \rho^2 z^{-2})$. The state space description of this structure is easily derived [3] and yields the realization matrix

$$\mathcal{R}_{\text{couple}} = \begin{bmatrix} \boldsymbol{A} & \boldsymbol{B} \\ \boldsymbol{C} & D \end{bmatrix} = \begin{bmatrix} \rho\cos\theta & -\rho\sin\theta & 1 \\ \rho\sin\theta & \rho\cos\theta & 0 \\ 0 & 1 & 0 \end{bmatrix}. \tag{9}$$

The inverse of this matrix is, with $m = \rho\sin\theta + \rho\cot\theta\cos\theta$

$$\mathcal{R}_{\text{couple}}^{-1} = \begin{bmatrix} \hat{\boldsymbol{A}} & \hat{\boldsymbol{B}} \\ \hat{\boldsymbol{C}} & \hat{D} \end{bmatrix} = \begin{bmatrix} 0 & 1/\rho\sin\theta & -\cot\theta \\ 0 & 0 & 1 \\ 1 & -\cot\theta & \rho\sin\theta + \rho\cot\theta\cos\theta \end{bmatrix}. \tag{10}$$

Fig. 8(b) shows a structure with this realization matrix and is therefore the causal dual of Fig. 8(a).

1) The Tapped Coupled Form: Fig. 9(a) shows the tapped coupled form. The tap coefficients D, c_1, and c_2 can be used to obtain arbitrary second-order numerators. The realization matrix and its inverse are

$$\mathcal{R}_{\text{tap}} = \begin{bmatrix} \rho\cos\theta & -\rho\sin\theta & 1 \\ \rho\sin\theta & \rho\cos\theta & 0 \\ c_1 & c_2 & D \end{bmatrix} = \begin{bmatrix} 1 & 0 & 0 \\ 0 & 1 & 0 \\ D & \alpha & \beta \end{bmatrix} \underbrace{\begin{bmatrix} \rho\cos\theta & -\rho\sin\theta & 1 \\ \rho\sin\theta & \rho\cos\theta & 0 \\ 0 & 1 & 0 \end{bmatrix}}_{\mathcal{R}_{\text{couple}}} \tag{11}$$

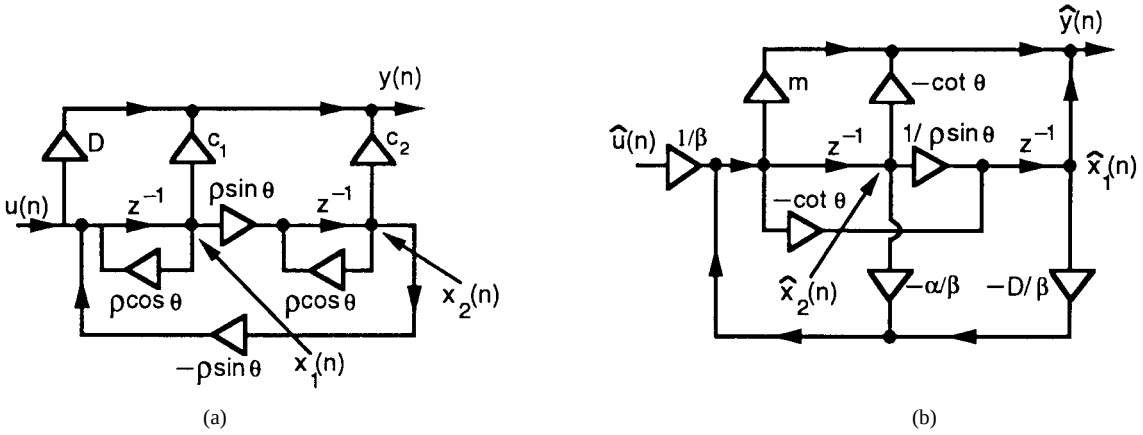

(a) (b)

Fig. 9. (a) Tapped coupled form. (b) Its causal dual.

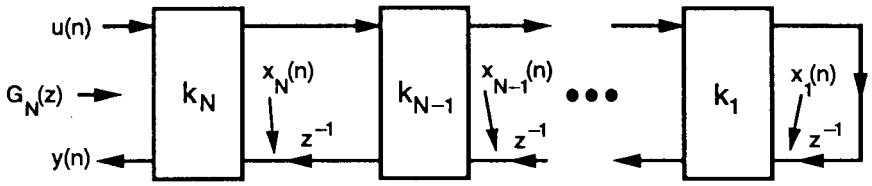

Fig. 10. General form of IIR allpass lattice structures.

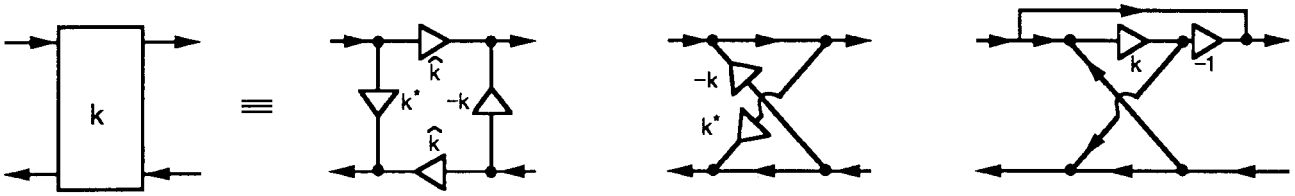

(a) (b) (c)

Fig. 11. Three possible cases of the IIR lattice section. (a) Normalized lattice. (b) Two-multiplier lattice. (c) One-multiplier, real-coefficient lattice.

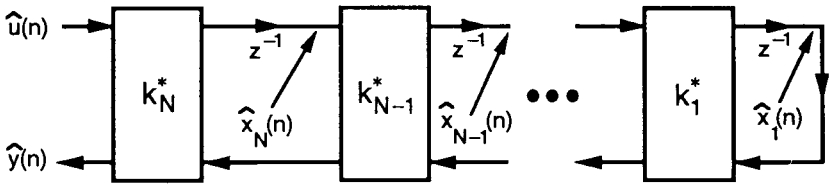

Fig. 12. Causal dual of the IIR lattice structure.

$$\mathcal{R}_{\text{tap}}^{-1} = \mathcal{R}_{\text{couple}}^{-1} \begin{bmatrix} 1 & 0 & 0 \\ 0 & 1 & 0 \\ D & \alpha & \beta \end{bmatrix}^{-1} = \mathcal{R}_{\text{couple}}^{-1} \begin{bmatrix} 1 & 0 & 0 \\ 0 & 1 & 0 \\ -D/\beta & -\alpha/\beta & 1/\beta \end{bmatrix} \tag{12}$$

where $\alpha = (c_1 - D\rho\cos\theta)/\rho\sin\theta$ and $\beta = c_2 + D\rho\sin\theta - \alpha\rho\cos\theta$. The structure for $\mathcal{R}_{\text{tap}}^{-1}$ can be obtained from that for $\mathcal{R}_{\text{couple}}^{-1}$ [i.e., from Fig. 8(b)] by replacing the input $\hat{u}(n)$ with the linear combination $[\hat{u}(n) - D\hat{x}_1(n) - \alpha\hat{x}_2(n)]/\beta$. This yields the causal dual shown in Fig. 9(b).

IV. Causal Duals for Lattice Structures

Fig. 10 shows the general form of the lattice structure for a causal Nth-order allpass filter $G_N(z) = Y(z)/U(z)$. The boxes labeled k_m can take several possible forms, three of which are shown in Fig. 11 (the one-multiplier section is applicable only for the real-coefficient case). The lattice coefficients k_m satisfy $|k_m| < 1$ so that $G_N(z)$ is stable, and $\hat{k}_m = \sqrt{1 - |k_m|^2}$ is real. The allpass function $G_N(z)$ depends on $\{k_m\}$ but not on which of the three building blocks is used.

The lattice structure with four-multiplier building blocks [Fig. 11(a)] is called the the *normalized structure* [12]. We will show that the causal dual is as in Fig. 12, where the boxes labeled k_m^* are the normalized building blocks of Fig. 11(a) with coefficients conjugated. Thus, the causal dual is obtained from the original structure by conjugating the multipliers and moving the delays from the bottom rails to the top rails. In the real coefficient case, the causal dual is identical to the original lattice except for delay movement.

We first show that the realization matrix $\hat{\mathcal{R}}_N$ of Fig. 12 is given by $\hat{\mathcal{R}}_N = \mathcal{R}_N^{-1}$, where $\mathcal{R}_N$ is the realization matrix of the normalized

lattice. Since it is well known that $\mathcal{R}_N$ is unitary for the normalized lattice [15], we only have to show that $\hat{\mathcal{R}}_N = \mathcal{R}_N^\dagger$ (transpose conjugate).

Lemma 1: The $(N+1)\times(N+1)$ realization matrix $\mathcal{R}_N$ for the lattice structure with normalized building blocks can be expressed as a product of N unitary matrices

$$\mathcal{R}_N = \begin{bmatrix} \boldsymbol{\Theta}_1 & \mathbf{0} \\ \mathbf{0} & \boldsymbol{I}_{N-1} \end{bmatrix} \begin{bmatrix} 1 & 0 & 0 \\ 0 & \boldsymbol{\Theta}_2 & 0 \\ 0 & 0 & \boldsymbol{I}_{N-2} \end{bmatrix} \begin{bmatrix} \boldsymbol{I}_2 & 0 & 0 \\ 0 & \boldsymbol{\Theta}_3 & 0 \\ 0 & 0 & \boldsymbol{I}_{N-3} \end{bmatrix} \cdots \begin{bmatrix} \boldsymbol{I}_{N-2} & \mathbf{0} & 0 \\ \mathbf{0} & \boldsymbol{\Theta}_{N-1} & 0 \\ 0 & 0 & 1 \end{bmatrix} \begin{bmatrix} \boldsymbol{I}_{N-1} & \mathbf{0} \\ \mathbf{0} & \boldsymbol{\Theta}_N \end{bmatrix}$$

where $\boldsymbol{\Theta}_m = \begin{bmatrix} -k_m & \hat{k}_m \\ \hat{k}_m & k_m^* \end{bmatrix}$ are 2×2 unitary matrices. ◇

Remark: This is consistent with the fact that unitary matrices can be factorized into (complex) planar rotations. However, the number of factors here is only N instead of the usual $N(N+1)/2$ [3].

Proof of Lemma 1: We use induction on the number of sections N. Consider Fig. 13, where an m-stage lattice is obtained by adding the mth section to the $(m-1)$-stage lattice. For the $(m-1)$-stage lattice, the input is $v_m(n)$, and the output is $x_m(n+1)$. With the mth stage added, the input and output of the system are defined as $v_{m+1}(n)$ and $x_{m+1}(n+1)$, respectively, and

$$\begin{bmatrix} v_m(n) \\ x_{m+1}(n+1) \end{bmatrix} = \begin{bmatrix} -k_m & \hat{k}_m \\ \hat{k}_m & k_m^* \end{bmatrix} \begin{bmatrix} x_m(n) \\ v_{m+1}(n) \end{bmatrix}. \tag{13}$$

Denoting the $m\times m$ realization matrix of the $(m-1)$-stage lattice as $\mathcal{R}_{m-1}$, we have

$$\begin{aligned} \text{States} \rightarrow \begin{pmatrix} x_1(n+1) \\ x_2(n+1) \\ \vdots \\ x_{m-1}(n+1) \end{pmatrix} \\ \text{Output} \rightarrow \begin{pmatrix} x_m(n+1) \end{pmatrix} \end{aligned} &= \mathcal{R}_{m-1} \begin{pmatrix} x_1(n) \\ x_2(n) \\ \vdots \\ x_{m-1}(n) \\ \hline v_m(n) \end{pmatrix} \\ &= \mathcal{R}_{m-1} \begin{pmatrix} \boldsymbol{I} & 0 & 0 \\ \mathbf{0} & -k_m & \hat{k}_m \end{pmatrix} \begin{pmatrix} x_1(n) \\ x_2(n) \\ \vdots \\ x_{m-1}(n) \\ x_m(n) \\ v_{m+1}(n) \end{pmatrix} \end{aligned} \tag{14}$$

using the first equation of (13). Append a row to this equation to indicate the new output $x_{m+1}(n+1)$

$$\begin{aligned} \text{States} \rightarrow \begin{pmatrix} x_1(n+1) \\ x_2(n+1) \\ \vdots \\ x_{m-1}(n+1) \\ x_m(n+1) \end{pmatrix} \\ \text{Output} \rightarrow \begin{pmatrix} x_{m+1}(n+1) \end{pmatrix} \end{aligned}$$

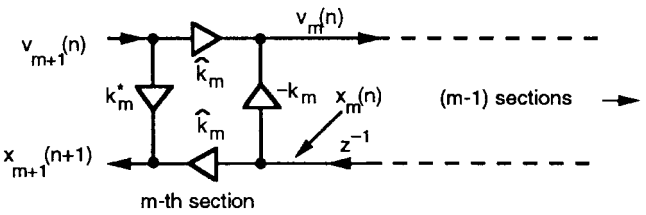

Fig. 13. Adding the mth section to the normalized IIR lattice.

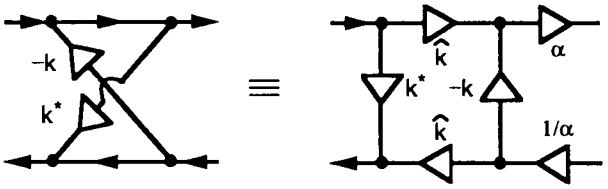

Fig. 14. Relation between the two types of IIR lattice sections.

$$= \underbrace{\begin{pmatrix} \mathcal{R}_{m-1} & 0 \\ \hline 0 & 1 \end{pmatrix} \begin{pmatrix} \boldsymbol{I} & 0 & 0 \\ 0 & -k_m & \hat{k}_m \\ 0 & \hat{k}_m & k_m^* \end{pmatrix}}_{\mathcal{R}_m} \cdot \begin{pmatrix} x_1(n) \\ x_2(n) \\ \vdots \\ x_{m-1}(n) \\ x_m(n) \\ \hline v_{m+1}(n) \end{pmatrix}. \tag{15}$$

This follows from the second equation in (13). Therefore, the realization matrices $\mathcal{R}_m$ and $\mathcal{R}_{m-1}$ are related as

$$\mathcal{R}_m = \begin{bmatrix} \mathcal{R}_{m-1} & \mathbf{0} \\ \mathbf{0} & 1 \end{bmatrix} \begin{bmatrix} \boldsymbol{I} & \mathbf{0} \\ \mathbf{0} & \boldsymbol{\Theta}_m \end{bmatrix}. \tag{16}$$

For $m=1$, we can explicitly verify that $\mathcal{R}_1 = \begin{bmatrix} -k_1 & \hat{k}_1 \\ \hat{k}_1 & k_1^* \end{bmatrix} = \boldsymbol{\Theta}_1$. It then follows from the preceding equation by induction that $\mathcal{R}_N$ has the form stated in the Lemma. ▽▽▽.

We can show similarly that the realization matrices for the m-stage lattice and $(m-1)$-stage lattice in Fig. 12 are related as

$$\hat{\mathcal{R}}_m = \begin{bmatrix} \boldsymbol{I} & 0 \\ 0 & \boldsymbol{\Theta}_m^* \end{bmatrix} \begin{bmatrix} \hat{\mathcal{R}}_{m-1} & 0 \\ 0 & 1 \end{bmatrix}$$

and that $\hat{\mathcal{R}}_1 = \boldsymbol{\Theta}_1^*$. Using this, we find that

$$\hat{\mathcal{R}}_N = \begin{bmatrix} \boldsymbol{I}_{N-1} & 0 \\ 0 & \boldsymbol{\Theta}_N^* \end{bmatrix} \begin{bmatrix} \boldsymbol{I}_{N-2} & 0 & 0 \\ 0 & \boldsymbol{\Theta}_{N-1}^* & 0 \\ 0 & 0 & 1 \end{bmatrix} \cdots \begin{bmatrix} \boldsymbol{I}_2 & 0 & 0 \\ 0 & \boldsymbol{\Theta}_3^* & 0 \\ 0 & 0 & \boldsymbol{I}_{N-3} \end{bmatrix} \begin{bmatrix} 1 & 0 & 0 \\ 0 & \boldsymbol{\Theta}_2^* & 0 \\ 0 & 0 & \boldsymbol{I}_{N-2} \end{bmatrix} \cdot \begin{bmatrix} \boldsymbol{\Theta}_1^* & 0 \\ 0 & \boldsymbol{I}_{N-1} \end{bmatrix}.$$

Therefore, $\hat{\mathcal{R}}_N = \mathcal{R}_N^\dagger = \mathcal{R}_N^{-1}$ (since $\boldsymbol{\Theta}_m^* = \boldsymbol{\Theta}_m^\dagger$), and Fig. 12 is the causal dual of the normalized lattice.

1) Denormalized Lattice Structures: The causal dual of the two-multiplier allpass lattice is also given by Fig. 12, where the building blocks marked k_m^* are two multiplier sections with k_m replaced by k_m^*.

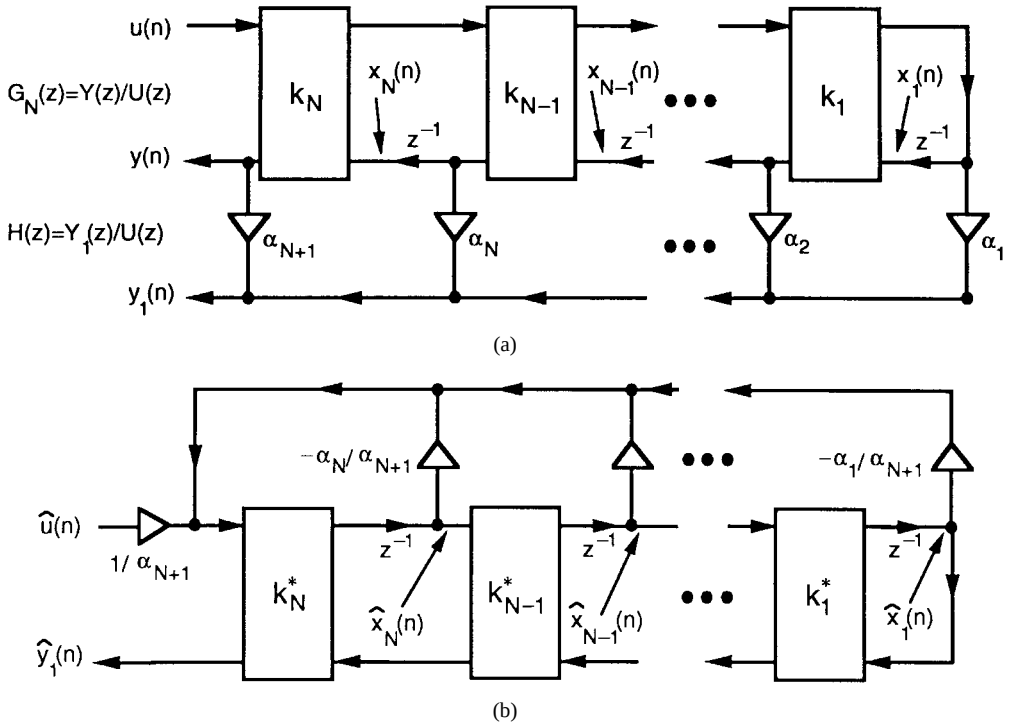

Fig. 15. (a) Tapped IIR lattice. (b) Its causal dual.

Proof: The two-multiplier and four-multiplier sections are schematically related as in Fig. 14, where $\alpha = 1/\hat{k}$ is real. Therefore, the state variables $x_m(n)$ of the four-multiplier structure and the state variables $x'_m(n)$ of the two-multiplier structure are related in a simple way. Thus, for fixed input $u(n)$, we can show after some work that $x'_m(n) = t_m x_m(n)$, where $t_m = \alpha_N \alpha_{N-1} \cdots \alpha_m$. Denoting the state space descriptions of the two- and four-multiplier lattices as $(\boldsymbol{A}_2, \boldsymbol{B}_2, \boldsymbol{C}_2, D_2)$ and $(\boldsymbol{A}_4, \boldsymbol{B}_4, \boldsymbol{C}_4, D_4)$, we have

$$\begin{bmatrix} \boldsymbol{A}_2 & \boldsymbol{B}_2 \\ \boldsymbol{C}_2 & D_2 \end{bmatrix} = \begin{bmatrix} \boldsymbol{T} & \boldsymbol{0} \\ \boldsymbol{0} & 1 \end{bmatrix} \begin{bmatrix} \boldsymbol{A}_4 & \boldsymbol{B}_4 \\ \boldsymbol{C}_4 & D_4 \end{bmatrix} \begin{bmatrix} \boldsymbol{T}^{-1} & \boldsymbol{0} \\ \boldsymbol{0} & 1 \end{bmatrix} \tag{17}$$

where $\boldsymbol{T}$ is diagonal with t_m on the diagonals. Inverting this, we obtain a very similar relation

$$\begin{bmatrix} \boldsymbol{A}_2 & \boldsymbol{B}_2 \\ \boldsymbol{C}_2 & D_2 \end{bmatrix}^{-1} = \begin{bmatrix} \boldsymbol{T} & \boldsymbol{0} \\ \boldsymbol{0} & 1 \end{bmatrix} \begin{bmatrix} \boldsymbol{A}_4 & \boldsymbol{B}_4 \\ \boldsymbol{C}_4 & D_4 \end{bmatrix}^{-1} \begin{bmatrix} \boldsymbol{T}^{-1} & \boldsymbol{0} \\ \boldsymbol{0} & 1 \end{bmatrix}. \tag{18}$$

Thus, the similarity transformation $\boldsymbol{T}$ that relates the two kinds of structures also relates their causal duals. We can arrive at the causal dual of the two multiplier structure simply by applying the diagonal transformation $\boldsymbol{T}$ to the causal dual of the normalized lattice. This is precisely Fig. 12 with the conjugated two-multiplier sections. For the one-multiplier lattice, a similar development shows that the causal dual is exactly identical to the original structure, except for the movement of the delay elements.

2) The Tapped Lattice Structure: This is shown in Fig. 15(a). The transfer function $H(z)$ now has denominator identical to that of the allpass filter $G_N(z)$. The tap coefficients α_n can always be chosen to realize the arbitrary numerator of $H(z)$. We will show that the causal dual of this is given by the structure of Fig. 15(b). (This assumes $\alpha_{N+1} \neq 0$. If $\alpha_{N+1} = 0$, the numerator of $H(z)$ has a smaller order than the denominator, an anticausal inverse does not exist [9], and the causal dual would then be of no interest.

For a given input $u(n)$, the state variables $x_i(n)$ in Fig. 15(a) are exactly identical to those in Fig. 10. Thus, the output of $H(z)$ is $y_1(n) = \Sigma_{i=1}^{N} \alpha_i x_i(n+1) + \alpha_{N+1} y(n)$, and the realization matrix $\mathcal{R}_{\text{arb}}$ for $H(z)$ is related to the realization matrix $\mathcal{R}_{\text{all}}$ of the allpass filter $G_N(z)$ as

$$\mathcal{R}_{\text{arb}} = \begin{bmatrix} \boldsymbol{I} & \boldsymbol{0} \\ \boldsymbol{a} & \alpha_{N+1} \end{bmatrix} \mathcal{R}_{\text{all}}$$

where $\boldsymbol{a} = [\alpha_1 \ \alpha_2 \ \cdots \ \alpha_N]$. Thus, the realization matrix of the causal dual is given by

$$\mathcal{R}_{\text{arb}}^{-1} = \mathcal{R}_{\text{all}}^{-1} \begin{bmatrix} \boldsymbol{I} & \boldsymbol{0} \\ -\boldsymbol{a}/\alpha_{N+1} & 1/\alpha_{N+1} \end{bmatrix}. \tag{19}$$

Now, $\mathcal{R}_{\text{all}}^{-1}$ is the realization matrix of the causal dual shown earlier in Fig. 12. Postmultiplication of $\mathcal{R}_{\text{all}}^{-1}$ as in the preceding equation means that we replace the system input with a new linear combination as shown by Fig. 15(b), which is therefore the causal dual of Fig. 15(a). This looks similar to the tapped lattice, but the taps are now used in feedback. This is consistent with the fact that the numerator of the original transfer function $H(z)$, which was determined by α_i, is now the denominator of the inverse. Whether this structure is stable depends on the numerator of $H(z)$ because the causal dual transfer function is $1/H(z^{-1})$.

V. Concluding Remarks

It is well known in digital filter literature that the coupled form and lattice structures have a further property called passivity that guarantees that they are free from zero-input limit cycles. It turns out that the same property is true for the causal duals of the lattice structures but not those of coupled form structures. A structure is said to be *passive* (see [13] and references therein) if the state transition matrix $\boldsymbol{A}$ satisfies $\boldsymbol{v}^\dagger \boldsymbol{A}^\dagger \boldsymbol{A} \boldsymbol{v} \leq \boldsymbol{v}^\dagger \boldsymbol{v}$ for all $\boldsymbol{v}$ and *strictly passive* $\boldsymbol{v}^\dagger \boldsymbol{A}^\dagger \boldsymbol{A} \boldsymbol{v} < \boldsymbol{v}^\dagger \boldsymbol{v}$ for $\boldsymbol{v} \neq \boldsymbol{0}$. In addition, $\boldsymbol{A}$ is said to be *generalized passive* if there exists a diagonal similarity transformation $\boldsymbol{T}$ such that $\boldsymbol{T}\boldsymbol{A}\boldsymbol{T}^{-1}$ is passive. For example, consider the matrix $\boldsymbol{A}$ for the direct-form structure (6). Unless the denominator of the transfer function has the form $1 + q_N z^{-N}$, the matrix $\boldsymbol{A}$ is not passive. The *limit cycle theorem* [13] says this. If we quantize only the state variables and

$$G(z) = \frac{D + z^{-1}(c_1 - 2\rho D\cos\theta) + z^{-2}(D\rho^2 - c_1\rho\cos\theta + c_2\rho\sin\theta)}{1 - 2\rho\cos\theta z^{-1} + \rho^2 z^{-2}.}$$

use only passive quantizers (i.e., devices which do not increase the magnitude), then the stability and generalized passivity of $\boldsymbol{A}$ ensures that there are no zero-input limit cycles. The coupled-form structure has a stricly passive $\boldsymbol{A}$, whereas all the lattice structures in Fig. 10 have $\boldsymbol{A}$ matrices, which are generalized passive [13]. Using this, the coupled form and lattice can be made free from zero input limit cycles.

For the causal dual of the normalized lattice, the realization matrix is $\mathcal{R}_N^{-1} = \mathcal{R}_N^{\dagger}$ since $\mathcal{R}_N$ is unitary. Therefore, $\hat{\boldsymbol{A}} = \boldsymbol{A}^{\dagger}$, showing that $\boldsymbol{A}^{\dagger}$ is generalized passive and stable. The same conclusion holds for the denormalized (e.g., two multiplier) lattice because it is related to the normalized system by a diagonal matrix [see (17)]. However, for the coupled-form structure, we show that the passivity of $\boldsymbol{A}$ does not imply that of the causal dual $\hat{\boldsymbol{A}}$. We saw that $\boldsymbol{A}$ has the form given in (9), and it is passive. The quantity $\hat{\boldsymbol{A}}$ depends on the choice of the output node $y(n)$. With $y(n)$ as indicated in Fig. 8(a), $G(z)$ is an all-pole filter, and its inverse is FIR. Since $\mathcal{R}^{-1}$ is as in (10), we have

$$\hat{\boldsymbol{A}} = \begin{bmatrix} 0 & 1/\rho\sin\theta \\ 0 & 0 \end{bmatrix}.$$

This matrix is not passive since it is possible that $1/\rho\sin\theta > 1$ (because $\rho < 1$ for stability). However, it is FIR, and we do not have limit cycles anyway. For a nontrivial example, consider the tapped coupled form of Fig. 9(a). The tap coefficients D, c_1, and c_2 allow us to obtain arbitrary numerators for the transfer function $G(z) = Y(z)/U(z)$. We can verify that the transfer function of this structure is as shown at the top of the page. Of interest here is the allpass function $G(z) = (\rho^2 - 2\rho\cos\theta z^{-1} + z^{-2})/(1 - 2\rho\cos\theta z^{-1} + \rho^2 z^{-2})$ for which tap coefficients are

$$D = \rho^2, c_1 = 2\rho(\rho^2 - 1)\cos\theta, \quad c_2 = \frac{1 - \rho^4 + 2\rho^2(\rho^2 - 1)\cos^2\theta}{\rho\sin\theta}. \tag{20}$$

The quantities α and β in the causal dual structure therefore simplify to the form $\alpha = (\rho^2 - 2)\cot\theta, \beta = 1/\rho\sin\theta$. Substituting into (12) and simplifying, we find that the matrix $\hat{\boldsymbol{A}}$ for the causal dual is

$$\hat{\boldsymbol{A}} = \begin{bmatrix} a_1 & a_2 \\ a_3 & a_4 \end{bmatrix} = \begin{bmatrix} \rho^3\cos\theta & \dfrac{1}{\rho\sin\theta} + \dfrac{\rho(\rho^2 - 2)\cos^2\theta}{\sin\theta} \\ -\rho^3\sin\theta & -\rho(\rho^2 - 2)\cos\theta \end{bmatrix}. \tag{21}$$

This matrix is not necessarily passive. For example, the element a_2 can exceed unity as θ gets close to zero. We will now show that $\hat{\boldsymbol{A}}$ may not even be generalized passive. That is, there may not exist a diagonal $\boldsymbol{T}$ such that $\boldsymbol{T}\hat{\boldsymbol{A}}\boldsymbol{T}^{-1}$ is passive. To see this, let

$$\boldsymbol{T} = \begin{bmatrix} 1 & 0 \\ 0 & t \end{bmatrix}$$

and compute

$$\boldsymbol{T}\hat{\boldsymbol{A}}\boldsymbol{T}^{-1} = \begin{bmatrix} a_1 & a_2/t \\ ta_3 & a_4 \end{bmatrix}.$$

The transformation $\boldsymbol{T}$ does not affect the diagonal elements a_1 and a_4. This matrix will fail to be passive (regardless of t) when $a_4^2 > 1$. For example, if $\rho^2 = 2/3$, then $a_4^2 = \rho^2(\rho^2 - 2)^2\cos^2\theta = (32/27)\cos^2\theta$, which exceeds unity for certain values of θ. In this case, therefore, $\hat{\boldsymbol{A}}$ is not generalized passive.

REFERENCES

[1] P. P. Vaidyanathan, P. Regalia, and S. K. Mitra, "Design of doubly complementary IIR digital filters using a singlecomplex allpass filter, with multirate applications," *IEEE Trans. Circuits Syst.*, vol. CAS-34, pp. 378–389 Apr. 1987.

[2] T. A. Ramstad, "IIR filterbank for subband coding of images," in *Proc. IEEE Int. Symp. Circuits Syst.*, Espoo, Finland, June 1988, pp. 827–830.

[3] P. P. Vaidyanathan, *Multirate Systems and Filter Banks.* Englewood Cliffs, NJ: Prentice-Hall, 1993.

[4] A. V. Oppenheim and R. W. Schafer, *Discrete-Time Signal Processing.* Englewood Cliffs, NJ: Prentice-Hall, 1989.

[5] J. Husoy and T. A. Ramstad, "Application of an efficient parallel IIR filter bank to image subband coding," *Signal Process.*, vol. 20, pp. 279–292, Aug. 1990.

[6] H. Babic, S. K. Mitra, C. D. Creusere, and A. Das, "Perfect reconstruction recursive QMF banks for image subband coding," in *Proc. 25th Annu. Asilomar Conf. Signals, Syst., Comput.*, Pacific Grove, CA, Nov. 1991.

[7] S. K. Mitra, C. D. Creusere, and H. Babic, "A novel implementation of perfect reconstruction QMF banks using IIR filters for infinite length signals," in *Proc. IEEE Int. Symp. Circuits Syst.*, San Diego, CA, May 1992, pp. 2312–2315.

[8] T. Chen and P. P. Vaidyanathan, "General theory of time-reversed inversion for perfect reconstruction filter banks," in *Proc. 26th Annu. Asilomar Conf. Signals, Syst., Comput.*, Pacific Grove, CA, Oct. 1992, pp. 821–825.

[9] P. P. Vaidyanathan and T. Chen, "Role of anticausal inverses in multirate filter-banks—Part I: System-theoretic fundamentals, and Part II: The FIR case, factorizations, and biorthogonal lapped transforms," *IEEE Trans. Signal Processing*, pp. 1090–1115, May 1995.

[10] C. D. Creusere, "PR modulated polyphase filter banks using time-reversed subfilters," Ph.D dissertation, Dept. Elec. Comput. Eng., Univ. Calif. Santa Barbara, 1993.

[11] A. H. Gray, Jr., "Passive cascaded lattice digital filters," *IEEE Trans. Circuits Syst.*, vol. CAS-27, pp. 337–344, May 1980.

[12] A. H. Gray, Jr. and J. D. Markel, "A normalized digital filter structure," *IEEE Trans. Acoust. Speech Signal Processing*, vol. ASSP-23, pp. 268–277, June 1975.

[13] P. P. Vaidyanathan and V. C. Liu, "An improved sufficient condition for absence of limit cyclesin digital filters," *IEEE Trans. Circuits Syst.*, vol. CAS-34, pp. 319–322, Mar. 1987.

[14] C. W. Barnes and A. T. Fam, "Minimum-norm recursive digital filters that are free of overflow limit cycles," *IEEE Trans. Circuits Syst.*, vol. CAS-24, pp. 569–574, Oct. 1977.

[15] P. P. Vaidyanathan, "The discrete-time bounded real lemma in digital filtering," *IEEE Trans. Circuits Syst.*, vol. CAS-32, pp. 918–924, Sept. 1985.